J|A|C|S
ARTICLES
Published on Web 10/21/2006

Optical Characterization of Eu-Doped and Undoped Gd_2O_3 Nanoparticles Synthesized by the Hydrogen Flame Pyrolysis Method

Ewa M. Goldys,*,† Krystyna Drozdowicz-Tomsia,† Sun Jinjun,† Dosi Dosev,‡ Ian M. Kennedy,‡ Sergiey Yatsunenko,§ and Marek Godlewski§

Contribution from the Division of Information and Communication Sciences, Macquarie University, Sydney 2109 NSW, Australia, Department of Mechanical and Aeronautical Engineering, University of California Davis, One Shields Avenue, Davis, California 95616, and Institute of Physics, Polish Academy of Sciences, Warsaw, AL Lotnikow 32/46, Poland

Received March 30, 2006; E-mail: goldys@ics.mq.edu.au

Abstract: Rare-earth-doped nanoparticles are promising materials for fluorescent labeling, as they are characterized by a high Stokes shift, narrow emission spectra, long lifetimes, minimized photobleaching, and low toxicity. We examined the structural and optical properties of europium-doped gadolinium oxide nanoparticles synthesized by the flame pyrolysis method, with specific emphasis on full spectral characterization and fluorescence kinetics. The emission−excitation characterization revealed the presence of predominantly monoclinic but also highly luminescent cubic phases with a prominent oxygen-to-europium charge-transfer band in the 230−260 nm range. A broad emission band in the visible region, corresponding to a similar band in undoped Gd_2O_3, related to the matrix surface defects, was observed in time-gated spectroscopy of doped nanopowders. All of the examined nanopowders showed very short decay components, on the order of 2 ns, and much longer millisecond decay times characteristic of lanthanide ions. At intermediate times, on the order of 20−100 ns, a complex behavior of the decay was observed, indicative of progressive energy transfer to the lanthanide ion, which varied with different intrashell transitions. Structural characterization data by means of XRD measurements allowed for unambiguous determination of the Eu:Gd_2O_3 crystallographic structure and cell dimensions to be consistent with a predominantly monoclinic phase.

1. Introduction

There is continuing interest in europium-activated phosphors for a variety of applications including X-ray imaging, field emission or electroluminescent displays, fiber-optic amplifiers, lasers, and waveguides. More recently, nanoparticles made of lanthanide oxides have been investigated as emerging materials for fluorescent labeling[1−3] due to their large Stokes shift, sharp emission spectra, long lifetime, flexibility of excitation wavelengths, suitability for multiphoton and up-conversion excitation, and reduced photobleaching. Nanoparticles with different emission wavelengths important for these applications can be obtained by controlled doping of lanthanide ions into appropriate host materials. Excitation of the lanthanide in such systems occurs via absorption of light by a coordinating crystal/ligand and subsequent transfer of its electronic energy to the emissive excited-state manifold of the lanthanide ion.

The electronic structure of the lanthanide ion in the most frequently occurring trivalent state consists of a common xenon core and a $4f^n$ shell, which is progressively filled through the series. Imperfect shielding of $4f^n$ electrons results in them being drawn inside of the $5s^25p^6$ closed shells of the xenon core, leading to the effect known as lanthanide contraction.[4] Consequently, such $4f^n$ electrons interact weakly with any external environment, and only a small crystalline Stark splitting of 4f levels takes place. As a result, absorption and emission spectra of lanthanide(III) ions appear as sharp, narrow bands, whose positions are very weakly dependent on the environment or crystal field. The fine structure of these bands can provide important information about the crystallography and position of lanthanide ions in such structures. It has to be noted that the studies of crystalline Stark splitting of 4f levels require special, site-selective excitation conditions.

In contrast with semiconductor quantum dots,[5,6] the emission wavelength of the lanthanide oxide nanoparticles is independent of the particle size, as the exciton Bohr radius in such materials is very small, and thus the nanoparticle size in the latter material is not critical for the spectral properties. At the same time, when lanthanide ions are incorporated into a nanosize medium, some

† Macquarie University.
‡ University of California Davis.
§ Polish Academy of Sciences.

(1) Gordon, W. O.; Carter, J. A.; Tissue, B. M. *J. Lumin.* **2004**, *108*, 339.
(2) Dosev, D.; Nichkova, M.; Liu, M.; Guo, B.; Liu, G.; Hammock, B. D.; Kennedy, I. M. *J. Biomed. Opt.* **2006**, *10*, 064006.
(3) Nichkova, M.; Dosev, D.; Gee, S. J.; Hammock, B. D.; Kennedy, I. M. *Anal. Chem.* **2005**, *77*, 6864.
(4) Kennedy, R. J.; Campbell, J. C. *J. Phys. C: Solid State Phys.* **1980**, *13*, 5341.
(5) Bruchez, M.; Maronne, M.; Gin, P.; Weiss, S.; Alivisatos, A. P. *Science* **1998**, *281*, 2013.
(6) Chan, W. C. W.; Nie, S. *Science* **1998**, *281*, 2016.

10.1021/ja0621602 CCC: $33.50

modification to their fluorescence and time decay characteristics may be expected due, for example, to the proximity to the surface and possible contribution of crystalline defects as well as increased sensitivity to the environment through donor−acceptor energy transfer. As lanthanide oxides are used as commercial phosphors, it can be predicted that biological labels based on these materials will have better photostability than the commercially available polystyrene nanoparticles doped with lanthanide chelates. Doped lanthanide oxide nanoparticles can be synthesized by a variety of techniques such as chemical vapor deposition (CVD), spray pyrolysis, pulsed laser deposition, and solution-based sol−gel methods. These processes are relatively simple, safe, and scalable for mass production.

In this work, we demonstrate the results of optical characterization for europium-doped gadolinium oxide (Gd_2O_3:Eu) nanoparticles with various Eu doping levels and crystallographic structure, produced by spray pyrolysis.

2. Experimental Section

Europium-doped Gd_2O_3 nanoparticles were synthesized by a spray pyrolysis method, described earlier.[7] As reagents, ethanol solutions containing nitrides of europium and gadolinium were used at the ratios required for the target doping levels. For example, to synthesize the 20% Eu:Gd_2O_3 nanoparticles studied here, we used ethanol solutions at concentrations of 20 mM $Eu(NO_3)_3$ and 80 mM $Gd(NO_3)_3$, and 30 mL of each solution was used.

The pyrolysis synthesis apparatus used in this work, described in detail in ref 7, consists of a special burner with several concentric nozzles. The reagents are delivered in liquid form to the center of the burner through a nebulizer. Air delivered to the burner at very high speed disperses the reagents into micrometer-size droplets, which are oxidized in the hydrogen diffusion flame. The flame temperature is measured with a thermocouple, and temperatures as high as 2100 °C are recorded. The reaction temperature can be adjusted to some extent by varying the flow ratios of hydrogen and air as well as the size of the droplets. The typical flow rates for the synthesis are 2 L/min for hydrogen and 2 L/min for air. The droplets formed in this system have a Gaussian size distribution with 80% of the droplets having diameters between 2 and 70 μm as previously reported.[7] The hydrogen diffusion flame serves as ignition for the spray flame that is formed by combustible ethanol droplets containing dissolved europium and gadolinium precursors. Nanoparticles are formed due to oxidation reaction that takes place within the flame. The nanoparticles are then collected thermophoretically on a coldfinger suspended above the flame. The production rate for this synthesis procedure is about 400−500 mg/h.

Assuming a 100 mmol solution of $Gd(NO_3)_3$, there are 4×10^{-16} mol of dissolved nitrate in a 2 μm droplet and 18×10^{-12} mol in a 70 μm droplet. The oxidation reaction that leads to the formation of M_2O_3 from $M(NO_3)_3$ (where M = Gd or Eu)[8] can be written as:

$$4M(NO_3)_3 \rightarrow 2M_2O_3 + 12NO_2 + 3O_2$$

Therefore, 2 mol of nitrate generates 1 mol of oxide, leading to between 4×10^{-16} and 1.8×10^{-11} mol of Gd_2O_3 product from droplets between 2 and 70 μm. Taking into account an overall molecular weight of Gd_2O_3 (362 g mol^{-1}), we calculate that the mass of the oxide particles from this range of droplet diameters falls between 5.8×10^{-19} and 2.5×10^{-14} g per particle. This corresponds to particle diameters between 5 and 185 nm, assuming a spherical shape with the density of Gd_2O_3.

We synthesized nanoparticles with 0%, 5%, 10%, 15%, and 20% of europium in Gd_2O_3. The as-synthesized nanoparticles were suspended in methanol in an ultrasonic bath for 30 min to break up any weak agglomerates formed during the collection process. The solution with dispersed nanoparticles was collected, and the sediments were discarded. The primary Eu:Gd_2O_3 particles synthesized by this method had a relatively broad size distribution from 2 to 300 nm, which is in agreement with the theoretically estimated particle sizes. The nanoparticle dimensions and size distribution were determined using a Phillips CM-12 TEM. Figure 1 shows the representative TEM image of Eu-doped Gd_2O_3 nanoparticles. The collected nanoparticles are not aggregated, and both small and large nanoparticles exhibit smooth morphology. They had an overall spherical shape, but close examination of images suggested that the larger particles were polycrystalline with multiple domains in the material.[9]

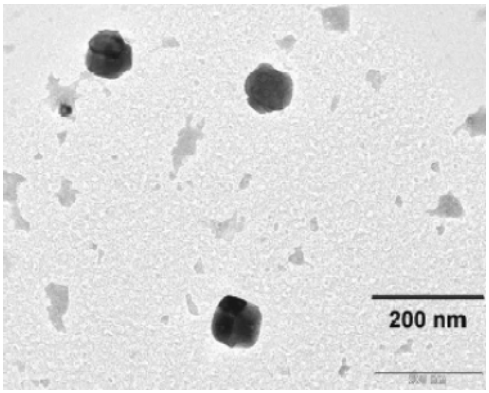

Figure 1. Bright-field TEM image of Eu:Gd_2O_3 nanoparticles synthesized by the spray pyrolysis method.

As-synthesized Eu:Gd_2O_3 nanoparticles without size selective centrifugation were used for X-ray diffraction (XRD) and optical characterization, either as dry powders or dispersed in methanol. For the confocal microscopy studies, small amounts of powder were placed on microscope slides, covered with refractive index matching liquid (glycerol), and sealed by a cover slip.

Continuous wave (CW) spectroscopic measurements were carried out using a Fluorolog 3 Tau 3 system from Jobin-Yvon-Horiba, with 450 W Xe lamp excitation. The spectra were corrected for system response, and all data were collected at room temperature. Laser-excited fluorescence was measured in a confocal laser-scanning microscope Leica TCM SP2 with spectral capabilities and 5 nm resolution provided by an acousto-optic beam splitting (AOBS) module.

Photoluminescence spectra were collected using the frequency doubled Spectra Physics DCR 2 YAG:Nd laser ($\lambda_{exc} = 532$ nm) as the excitation source, a Spex 1269 1.26 m monochromator and a Hamamatsu R928P photomultiplier (cooled to −30 °C), or Hammamatsu CCD detectors. Photoluminescence kinetics was recorded in the same setup, using a gated photon counter model SR400 from Stanford Research Systems as a boxcar. The laser modulation frequency and pulse duration were 30 Hz and 1 ns, respectively. We collected the spectra at 2 ns intervals for up to 8196 ns in the entire 550−730 nm emission range with 0.4 nm resolution on a Hammamatsu CCD photodetector. The crystal structure of the nanoparticles was verified by means of X-ray diffraction using an Inel XRG3000 X-ray diffractometer.

3. Results and Discussion

3.1. CW Spectroscopy of Eu-Doped and Undoped Gd_2O_3 Nanoparticles. First, we present the results of measurements for the 10% Eu:Gd_2O_3 nanoparticles dispersed in methanol. Figure 2 shows the emission spectra taken at a range of excitation wavelengths of 350, 361, 378, 393, 405, 413, and 465 nm with spectral resolution of 5 nm, where the fluorescence

(7) Dosev, D.; Guo, B.; Kennedy, I. *J. Aerosol Sci.* **2006**, *37*, 402.
(8) Shikao, S.; Jiye, W. *J. Alloys Compd.* **2001**, *327*, 82.
(9) Dosev, D.; Guo, B.; Kennedy, I. M. *J. Aerosol Sci.* **2006**, *37*, 402.

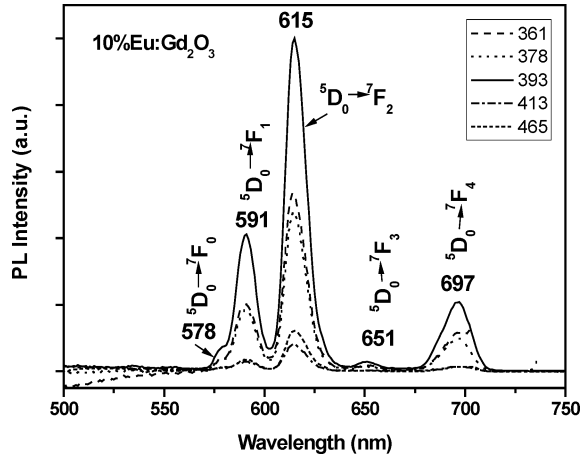

Figure 2. Emission spectra of 10% Eu:Gd_2O_3 nanoparticles suspended in methanol taken at a range of excitation wavelengths of 361, 378, 393, 413, and 465 with spectral resolution of 5 nm. In these spectra, the fluorescence and Raman signals of methanol have been subtracted.

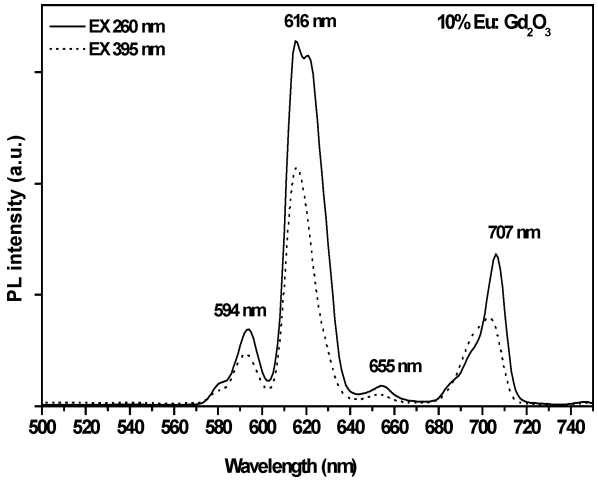

Figure 3. Emission spectra of 10% Eu:Gd_2O_3 nanoparticles taken at excitation wavelengths of 260 and 395 nm with spectral resolution of 5 nm.

and Raman signals of methanol have been subtracted. All nanoparticles spectra have a similar character with characteristic fluorescence bands corresponding to Eu^{3+} f−f transitions. These are dominated by the transition identified as $^5D_0-^7F_2$ with maximum around 615 nm. The remaining bands in order of decreasing intensity have been assigned as $^5D_0-^7F_1$ at 591 nm, $^5D_0-^7F_4$ at 697 nm, $^5D_0-^7F_0$ at 578 nm, and finally $^5D_0-^7F_3$ at 651 nm. At all excitation wavelengths, the fluorescence peaks have an approximately Gaussian shape.

Figures 3 and 4 show the emission spectra taken for 10% Eu and 15% Eu:Gd_2O_3 nanoparticles, respectively, with the nanoparticles directly placed between two quartz slides. At 260 nm excitation wavelength, we observe the splitting of the $^5D_0-^7F_2$ emission into two bands with maxima at 615 and 622 nm and a significant change in shape and position of the $^5D_0-^7F_4$ band, which no longer resemble a single Gaussian. In both 10% Eu and 15% Eu:Gd_2O_3 samples, its maximum is red-shifted to 706 nm, as compared to the emission for 10% Eu:Gd_2O_3 nanoparticles dispersed in methanol. Other transitions are only slightly red-shifted (by about 3 nm) as compared to measurements in methanol; the peaks are observed at 594, 694, and 581 nm for $^5D_0-^7F_1$, $^5D_0-^7F_4$, and $^5D_0-^7F_0$ transitions, respectively, and the shapes are Gaussian. Interestingly, at 395 nm excitation,

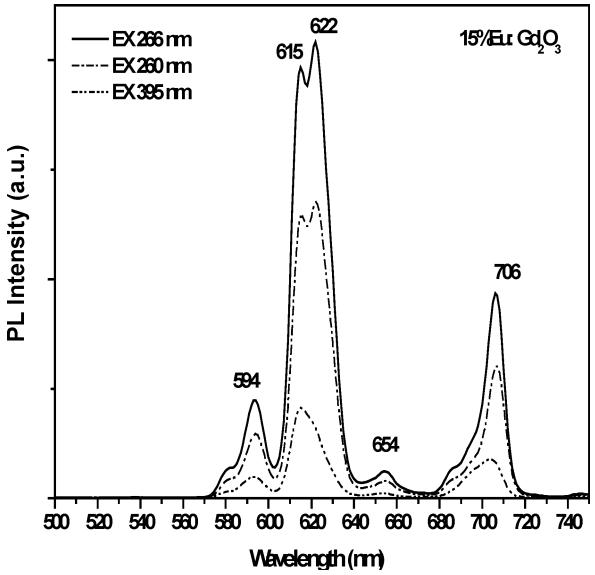

Figure 4. Emission spectra of 15% Eu:Gd_2O_3 nanoparticles taken at excitation wavelengths of 260, 266, and 395 nm with spectral resolution of 5 nm.

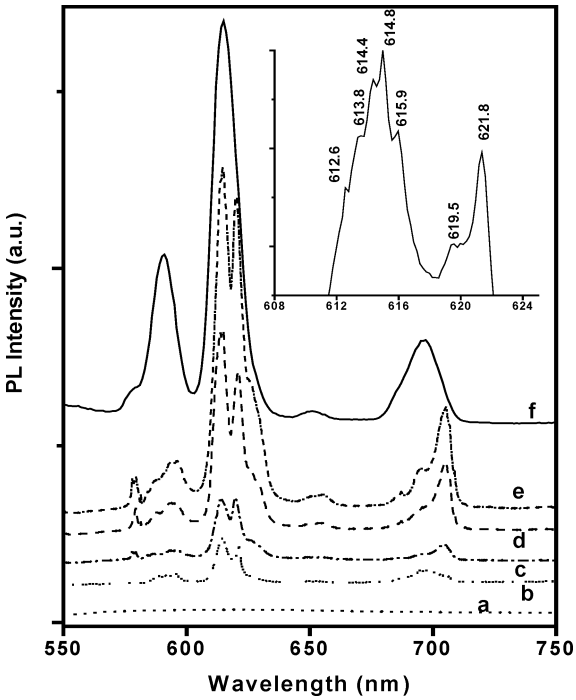

Figure 5. Emission spectra of pure and Eu-doped Gd_2O_3 monoclinic nanoparticles with various Eu doping levels: 0% (a), 5% (b), 10% (c), 15% (d), and 20% (e) with 532 nm excitation. (The spectra were shifted for clarity.) Emission spectra of cubic 10% Eu:Gd_2O_3 nanoparticles excited at 465 nm (f). Inset shows the enlarged $^5D_0-^7F_2$ transition region for 5% Eu:Gd_2O_3 monoclinic nanoparticles.

the spectra of dry powders appear very similar to those measured in methanol for both 10% Eu and 15% Eu nanoparticles, and the red shift is not observed.

Next, we present the results of room-temperature (RT) photoluminescence measurements for a range of samples prepared in the same way as in Figures 3 and 4, but with varying Eu doping levels in the 5−20% range, all excited at 532 nm by the frequency doubled Nd:YAG laser. These emission spectra are shown in Figure 5a−e. In the same graph, the emission spectrum (Figure 5f) with a Xe lamp excitation at 465 nm for

the 10% Eu:Gd_2O_3 sample dispersed in methanol is presented for comparison. All samples excited at 532 nm show very complex spectra with intensity of emission increasing proportionally with the increase of the europium content up to 20% of Eu in Gd_2O_3. For 5% Eu:Gd_2O_3, within the $^5D_0-^7F_2$ transition, the emission peaks at 612.6, 613.8, 614.4, 614.8, 615.9, 619.5, and 621.8 nm are observed (see inset of Figure 5). The splitting of the spectra for 532 nm laser excitation and 260 nm Xe lamp excitation (Figures 3 and 4) and its absence previously noted for the nanoparticles suspended in methanol suggest that the nanoparticles synthesized by the pyrolysis method are polycrystalline (Figure 1) with predominantly monoclinic crystallites, whose fluorescence from monoclinic form is totally quenched in methanol. The absence of splitting is typical for Eu^{3+} ions in the cubic structure of lanthanide oxides. In such structures, Eu^{3+} ions are located in two crystallographically nonequivalent sites with 6-fold coordination: one possessing C_2 point symmetry (with Eu^{3+} in the center of a distorted cube with two oxygen vacancies on the face diagonal) and an S_6 site symmetry (with inversion symmetry resulting from two oxygen vacancies lying on one body diagonal). In Gd_2O_3, 75% Gd^{3+} ions occupy the C_2 sites, and 25% Gd^{3+} ions occupy the S_6 sites.[10,11] In the cubic structures, the emission mainly originates from the C_2 site, because this site has a statistically higher occupancy level and no center of inversion, and as a result the splitting of the spectra is not observed. In the monoclinic configuration, there are three nonequivalent point sites of Eu^{3+} usually referred to as A, B, and C, each of them of C_s symmetry. In such sites, Eu^{3+} is in seventh fold coordination. The coordination of two Eu^{3+} ions can be described by six oxygens at the apexes of a trigonal prism with a seventh oxygen atom along a normal to the face. The third Eu^{3+} ion is in the middle of a distorted octahedron with the seventh oxygen at a long distance.[12,13] Rare-earth oxides are able to crystallize into different polymorphic structures, but only one is stable. Both Gd_2O_3 and Eu_2O_3 crystallize in the cubic phase at low temperatures and invert directly and irreversibly to the monoclinic phase if held at 1570 and 1670 K, respectively, for an hour.[14] The flame temperature in our synthesis significantly exceeds these transition temperatures, and therefore both cubic and monoclinic structures for Eu:Gd_2O_3 can be expected.

The emission from europium in different sites in monoclinic Gd_2O_3 was studied by Dexpert-Ghys et al. (ref 15) and Daly and Schmidt (ref 16). In the case of non-site-selective excitation, used here, pronounced Stark splitting originating from the A, B, and C sites is not observed, but the lines at 621.8, 615.9, and 614.4 are the closest to those reported in refs 15 and 16, and can be interpreted as emissions from the A, B, and C sites of the monoclinic Eu:Gd_2O_3. It should be noted that our RT line positions are slightly different from those in ref 15 (where the spectra were collected at 4 K) and those in ref 16 (at 80 K) and small position differences of the emission lines are attributed

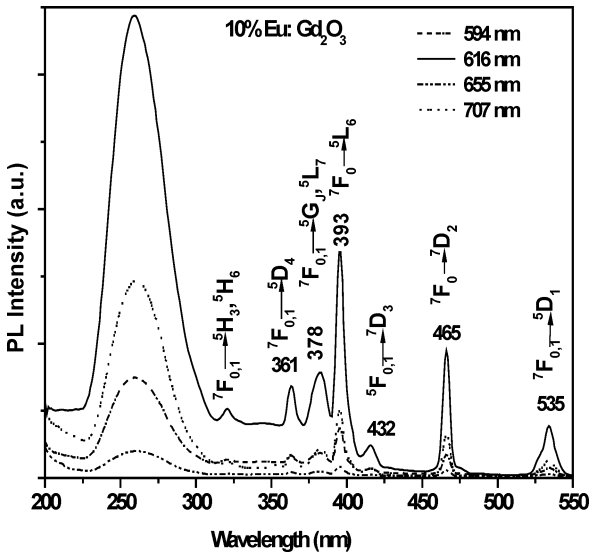

Figure 6. Excitation spectra of 10% Eu:Gd_2O_3 nanoparticles measured at the Eu emission lines of 594, 616, 655, and 707 nm.

to these variations in measurement conditions. This is also confirmed by the presence of sharp lines at 578.1, 579.4, and 581.5, which are in agreement with the A, B, and C emission lines for the $^5D_0-^7F_0$ transitions.[15,16] As the emission spectra for 10% Eu:Gd_2O_3 nanoparticles dispersed in methanol, shown previously in Figure 1, are characteristic for a pure cubic phase, we postulate that the emission from the monoclinic structures is much more susceptible to environmental factors. It thus becomes more easily quenched than in the cubic structures, and its emission intensity is strongly dependent on excitation wavelength.

Further, we characterized the excitation spectra of the nanoparticles. These were collected at the emission wavelengths of 594, 616, 655, and 707 nm, characteristic of the f−f emission bands in monoclinic structures (Figure 6). For emission wavelengths characteristic for the cubic structure (not shown here), the excitation bands with the same shape and position were observed. The spectrum in Figure 6 consists of a strong, narrow band centered at 230 nm and several sharp, weaker lines with maxima at 326, 361, 378, 393, 432, 465, and 535 nm. The band centered at 230 nm is due to the charge-transfer band (oxygen to europium),[17] whereas the sharp lines correspond to direct excitation of the europium f electrons. Because the spectrum has been recorded at room temperature, the transition from the $^7F_1$ state located 32.7 meV[17] above the $^7F_0$ ground state is also observed. This spectrum indicates that the most efficient excitation of the nanoparticles can be achieved in the 250−270 nm range. Pang et al. (ref 17) in a similar excitation experiment observed a much broader intense band in nanocrystaline Eu:Gd_2O_3 with a maximum at 230 nm and a shoulder at 250 nm, whose intensity increased with annealing temperature in the 500−900 °C temperature range. They also attributed the 230 nm band to the Gd_2O_3 host excitation band and the shoulder at 250 nm to the charge-transfer band between O^{2-} and Eu^{3+}. In our case, these two bands merge, presumably because of better crystalline structure formed in the high-temperature synthesis method. This merged band enables the most efficient

(10) Antic-Fidancev, E.; Holsa, J.; Lastusaari, M. *J. Alloys Compd.* **2002**, *341*, 82.
(11) Antic-Fidancev, E.; Hols, J.; Lastusaari, M. *J. Phys.: Condens. Matter* **2003**, *15*, 863.
(12) Holsa, J.; Leskela, T.; Leskela, M. *Inorg. Chem.* **1985**, *24*, 1539.
(13) Rice, D. K.; DeShazer, L. G. *J. Chem. Phys.* **1970**, *52*, 172.
(14) Roth, R. S.; Schneider, S. J. *J. Res. Natl. Bur. Stand. (U.S.)* **1960**, *A64*, 309.
(15) Dexpert-Ghys, J.; Faucher, M.; Caro, P. *Phys. Rev. B* **1981**, *23*, 607.
(16) Daly, J. G.; Schmidt, J. A.; Gruber, J. B. *Phys. Rev. B* **1983**, *27*, 5250.
(17) Pang, M. L.; Lin, J.; Fu, J.; Xing, R. B.; Luo, C. X.; Han, Y. C. *Opt. Mater.* **2003**, *23*, 547.

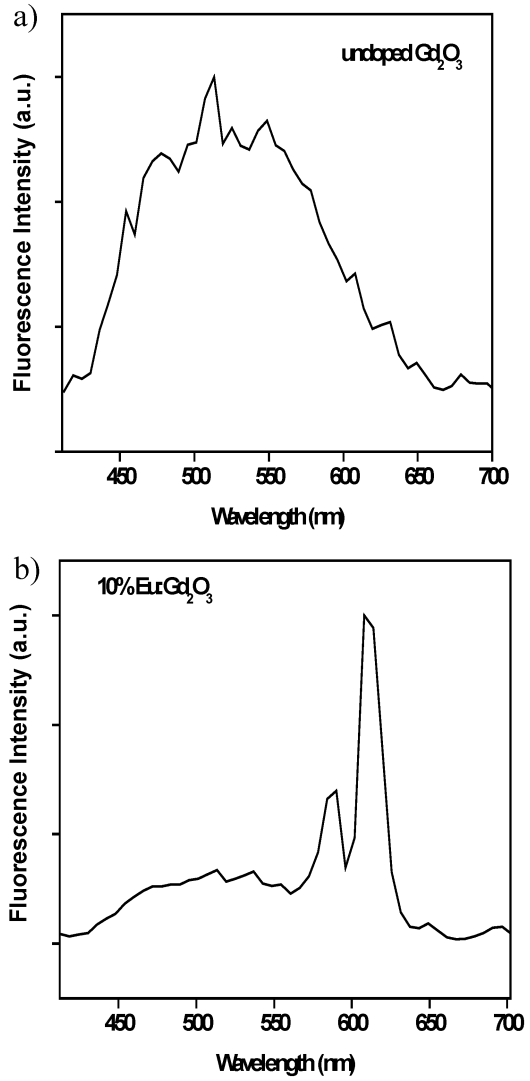

Figure 7. Emission spectra of (a) undoped Gd_2O_3 nanoparticles, and (b) 10%Eu:Gd_2O_3 nanoparticles, collected using 405 nm diode laser excitation. The spectra were taken in the Leica confocal microscopy system equipped with an AOBS at 5 nm resolution.

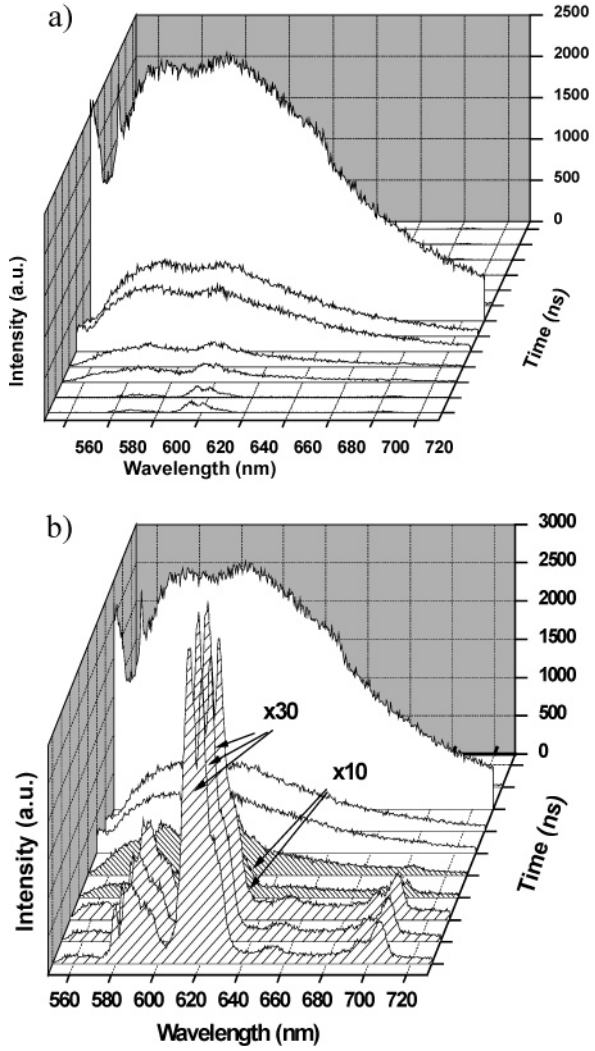

Figure 8. Time-resolved emission spectra of 10% Eu:Gd_2O_3 nanoparticles excited using pulsed laser excitation at 532 nm: (a) as collected spectra plotted at various time intervals, and (b) enlarged spectra for closer inspection.

energy transfer from the Gd_2O_3 host to the Eu^{3+} ions and the most efficient excitation of the nanoparticles.

Further, the synthesized undoped and doped Eu:Gd_2O_3 nanoparticles were characterized in a confocal microscopy system used for studies of biological fluorescence. We present the standard emission spectra acquired under laser excitation conditions, using a pulsed laser diode at 405 nm. The well-resolved emission peaks are shown in Figure 7b, and they correspond to the $^5D_0-^7F_{1,2}$ transitions discussed previously. In this case, the characteristic splitting in the monoclinic phase could not be observed due to acusto-optic beam splitter resolution limit of 5 nm. It has to be noted that the spectra in this case are collected from small agglomerates of nanoparticles dispersed in glycerol, which could have some quenching properties. For reference, we also took similar data of pure Gd_2O_3 nanoparticles (Figure 7a), which show a broad band centered at 530 nm.

Summarizing, we have spectroscopically characterized Eu:Gd_2O_3 nanoparticles with doping levels in the 5−20% Eu range. We have interpreted the observed emission and excitation bands and attributed them to corresponding f−f transitions in predominantly monoclinic Eu:Gd_2O_3 nanoparticles.

3.2. Time-Resolved Measurements. In the time-resolved fluorescence measurements reported here, the time-dependent fluorescence signal excited by a nanosecond laser pulse is collected for a variety of emission wavelengths in the examined range. The resulting three-dimensional plots of temporal evolution of fluorescence emission for Gd_2O_3 nanoparticles with 10% Eu excited at 532 nm are shown in Figure 8a,b. These show the representative spectra collected at increasing time intervals following the excitation pulse. Initially, a very broad and intense emission is observed (shown here 30 ns after the excitation pulse), which we tentatively assign to photoluminescence originating from defect impurities or surface states in the Gd_2O_3 matrix and further refer to as the excited Gd_2O_3 matrix. It has been recently shown that band gap of Gd_2O_3 cubic nanoparticles doped with 5% Eu^{3+} ions slightly increase from 5.4 to 5.55 eV as the particle diameter is reduced from 50 to 7 nm,[18] and, at 532 nm excitation, such a matrix should be transparent. At

(18) Rivotzki, K.; Meyssamy, H.; Kornowski, A. M. *J. Phys. Chem. B* **2000**, *104*, 2824.

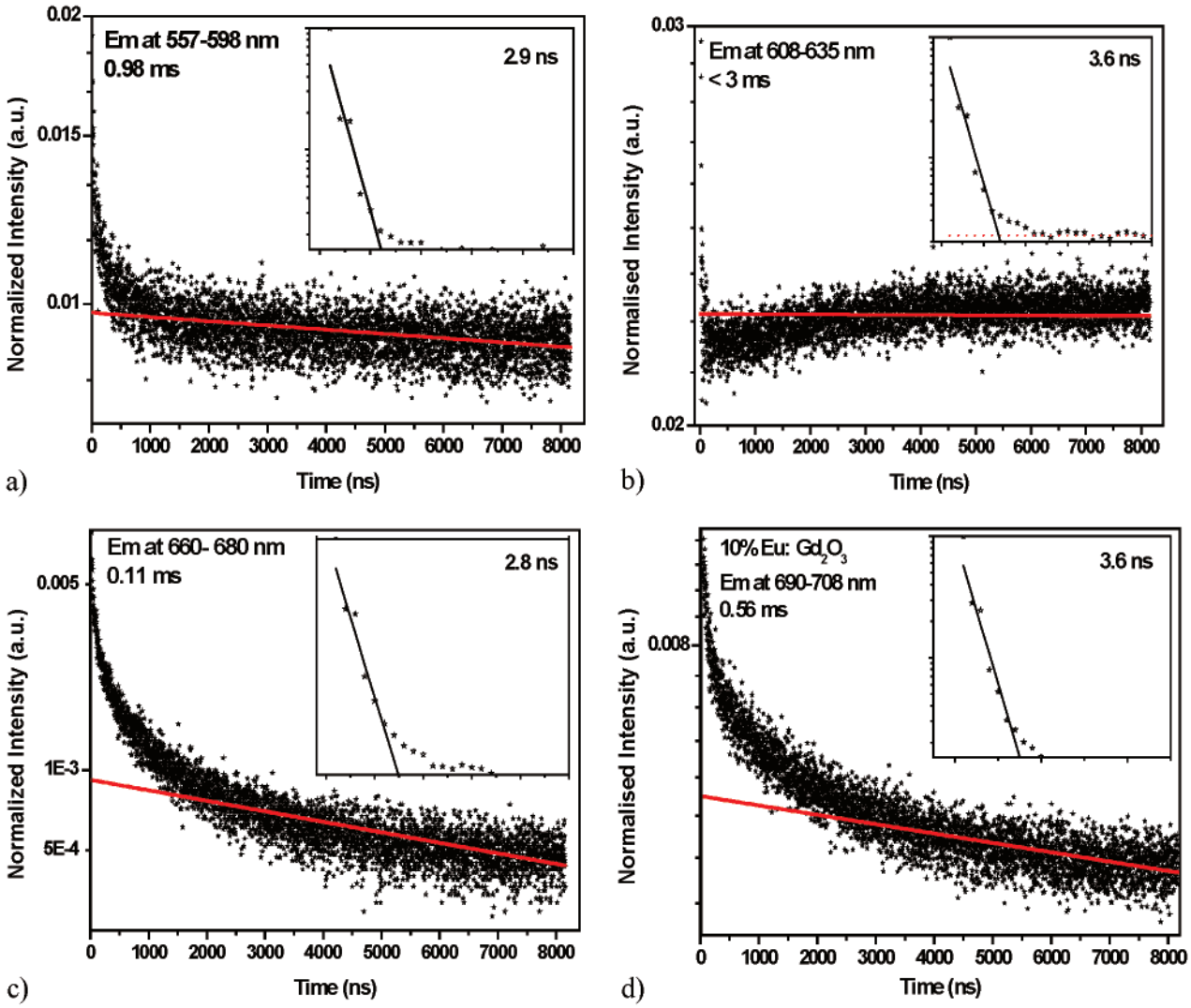

Figure 9. The decay curves of 10% Eu:Gd_2O_3 nanoparticles excited at 532 nm laser pulse (extracted from time-resolved emission spectra matrix) for the (a) 557−598 nm emission range, (b) 608−635 nm emission range, (c) 660−680 nm emission range, and (d) 690−708 nm emission range. For each graph, the long exponential decay component has been drawn as a red line. Insets in the (a), (b), (c), and (d) graphs show exponential fits for the short decay component.

higher 10% Eu doping levels investigated here, higher levels of defects can be expected. This emission decays very rapidly, and after further 6 ns its integrated emission intensity decreases 16 times as compared to the maximum integrated emission in this band. At higher delay times, the Eu^{3+} f−f transitions become visible; these are dominated by the most intense $^5D_0-{}^7F_2$ transition band centered at 618 nm. The sample studied shows a predominantly monoclinic phase, and as the band $^5D_0-{}^7F_2$ is split for this phase, three emission peaks at 616, 623, and 626 nm characteristic of the A, B, and C Eu^{3+} sites can be clearly observed. These are illustrated in Figure 8b. The shape of this emission is unchanged in the spectra at longer intervals, but its intensity decreases.

The same data can be analyzed by averaging the fluorescence decays over selected spectral ranges, and the results are shown in Figure 9a−d for the wavelength ranges shown in the figures. The fluorescence emission in Figure 9a was collected in the region 557−598 nm. In this spectral region, other authors have observed several $^5D_0-{}^7F_{0,1}-Eu^{3+}$ transitions. In monoclinic Gd_2O_3 with 5% Eu, the $^5D_0\rightarrow{}^7F_1$(A) transition at 601.3 nm and with decay time of 1.38 ns has been reported, as well as $^5D_0\rightarrow{}^7F_1$(C) transition at 594.0 nm and with a 0.78 ms decay time (ref 16). Other sources give the $^5D_0$ decay times of 1.6, 0.8, and 0.8 ms for the A, B, and C sites in bulk materials and 4.2, 2.8, and 3.2 ms for nanoparticles in the 8−17 nm size range for monoclinic Eu:Y_2O_3 (ref 20). It has to be noted that these data were acquired using site-selective resonant excitation. Our data show two characteristic decay times, a short, 2.9 ns decay (see Figure 9a, inset) as well as a long exponential decay tail with a lifetime of 0.98 ms, which is close to the 0.78 ms observed for $^5D_0\rightarrow{}^7F_1$(C).[16] The two parts of the decay curve are joined by an intermediate region, which could not be fitted by the sum of these two exponentials. A similar region is also apparent in the remaining decay characteristics (Figure 9b−d).

The fluorescence decay presented in Figure 9b was accumulated in the range 608−635 nm, where the most intense $^5D_0\rightarrow{}^7F_2$ transitions are observed with peaks at 616, 623, and 626 nm. This curve is nonexponential, but also shows a fast exponential decay component of 3.6 ns. At longer time delays,

(19) Mercier, B.; Dujardin, C.; Ledoux, G.; Louis, C.; Tillement, O. *J. Appl. Phys.* **2004**, *96*, 650.
(20) Williams, D. K.; Yan, H. B. M. *J. Lumin.* **1999**, *297*, 83.

the fluorescence intensity passes through a minimum at a few hundred nanoseconds, and progressively increases in a region to 4000 ns where it starts to decay at a slower rate. Such buildup of the decay curves was observed earlier (refs 18, 21) and was associated with a cross relaxation from $^5D_1$ to $^5D_0$ and with the well-known $Eu^{3+}(S_6)-Eu^{3+}(C_2)$ energy-transfer processes (ref 22). For the monoclinic phase, we postulate that $Eu^{3+}(A)-Eu^{3+}$-$(B)-Eu^{3+}(C)$ energy transfer becomes possible. We also note that the decreasing part of the fluorescence decay can be fitted to an exponential with a 3 ms decay time. This value describes only a net outcome of the radiative recombination and energy transfer, so its physical meaning cannot be simply interpreted, but is in good agreement with the averaged decay times measured for the A, B, and C sites for monoclinic $Eu:Y_2O_3$ nanoparticles. The behavior of fluorescence decay in the intermediate region observed in Figure 9a can also be attributed to similar energy-transfer processes, occurring at a faster scale, of hundreds of nanoseconds. We tentatively propose that the transfer occurs from the excited Gd_2O_3 matrix. It cannot be ruled out that the excited matrix, in addition to the nanosecond decay time, also has a second longer contribution, which cannot be separated from the energy transfer and $^5D_0 \rightarrow {}^7F_2$ decay characteristics. Pres et al. (ref 23) observed that lifetimes for $^5D_0 \rightarrow {}^7F_2$ transition for their cubic Gd_2O_3 particles increased from about 1.25 to 1.5 ms as a doping concentration was raised from 1% to 5% Eu, but experimental decay characteristics were not presented. Figure 8c shows the fluorescence decay collected in the region 660−680 nm, where only very weak $^5D_0 \rightarrow {}^7F_3$ transitions take place, but could not be clearly observed under our excitation conditions. Once again, we observe a short decay time of 2.8 nm as well as an intermediate region and an exponential tail with a decay time of 0.11 ms. This second, longer decay time we also attribute to the broad fluorescence band arising from the matrix.

Finally, Figure 9d shows the emission collected over the range 690−708 nm, where the transition $^5D_0 \rightarrow {}^7F_4$ is observed, at 697 nm. Again, the same pattern is observed with a fast decay time of 3.6 ns, followed by an intermediate region and an exponential decay tail with a lifetime of 0.56 ms.

Relatively good agreement in the observed short decay component for all measured wavelength ranges suggests that it originates from the same source, whose identity could not be established. The presence of a similar emission band observed at short intervals from the excitation pulse in the time-resolved measurements for doped and (in confocal microscopy measurements) for pure Gd_2O_3 nanoparticles links the short decay component to the defects or surface states in the Gd_2O_3 matrix. Long decay components of 0.98, 3, 0.11, and 0.56 ms estimated for the 557−598, 608−635, 660−680, and 690−708 nm spectral ranges, respectively, are the final result of the Eu^{3+} ion emission and energy-transfer processes.

3.3. Structural Characterization. XRD measurements were carried out to confirm cubic or monoclinic properties of characterized $Eu:Gd_2O_3$ nanoparticles. The measured XRD spectrum in the range of angles (2θ) between 28° and 33° for the 10% $Eu:Gd_2O_3$ nanoparticles is presented in Figure 10. It has low background level and strong peaks that unambiguously match the ref 24 and JCPDS database (JCPDS − International Centre for Diffraction Data) for the monoclinic Gd_2O_3. The absence of a peak around 28.6° characteristic for the (222) reflection of Gd_2O_3 in the cubic phase demonstrates that the content of this phase is negligible in this sample. In addition, the absence of peaks at 32.2°, 31.4° (typical for monoclinic Eu_2O_3) and 28.4°, 32.9° (typical for cubic Eu_2O_3) provides important evidence that there is efficient doping of the Eu ions into the Gd_2O_3 crystal without phase segregation. A very small difference of 0.9% in ionic radiuses of gadolinium and europium[25] makes Gd_2O_3 the most suitable matrix for incorporation of highly luminescent europium. The cell dimensions were calculated using the following relation between Bragg diffraction spacing and monoclinic cell parameters:

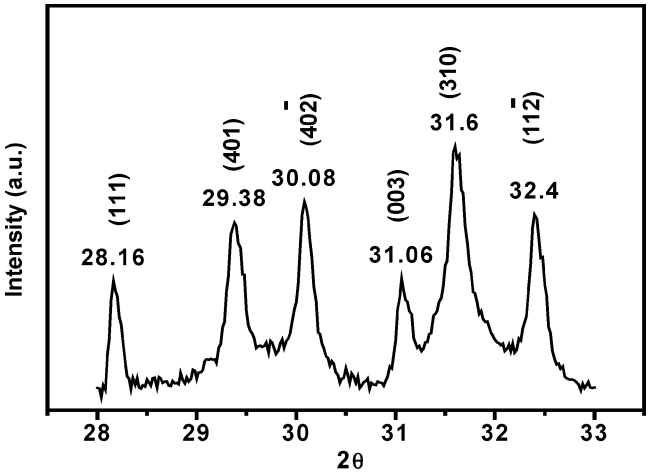

Figure 10. XRD spectrum of 10% $Eu:Gd_2O_3$ nanoparticles. Each peak has been assigned its angular position and corresponding reflection plane (in brackets).

Table 1. XRD Line Positions for Monoclinic Gd_2O_3

hkl	d_{calc}	$d_{observed}$
111	3.1585	3.1662
$40\bar{1}$	3.0332	3.0374
$40\bar{2}$	2.9647	2.9683
003	2.8747	2.8768
310	2.8216	2.8289
$11\bar{2}$	2.7549	2.7609

$$\frac{1}{d_{hkl}^{\,2}} = \frac{1}{\sin^2\beta} * \left(\frac{h^2}{a^2} + \frac{k^2 \sin^2\beta}{b^2} + \frac{l^2}{c^2} - \frac{2hl\cos\beta}{ac} \right) \quad (1)$$

where d_{hkl} is the Bragg diffraction spacing for the (*hkl*) plane, *h*,*k*,*l* are Muller indices, *a*,*b*,*c* are monoclinic cell dimensions, and β is the monoclinic cell angle.

The observed and calculated according to eq 1 positions of XRD lines are given in Table 1 and are consistent with the following cell dimensions as determined by a least-squares method: $a = 14.061 \pm 0.013$, $b = 3.566 \pm 0.006$, $c = 8.760 \pm 0.007$ Å, and $\beta = 100.10 \pm 0.08°$.

4. Conclusions

We have investigated the optical and structural properties of undoped and europium-doped Gd_2O_3 nanoparticles with differ-

(21) Seo, S. Y.; Sohn, K.-S.; Park, H. D.; Lee, S. *J. Electrochem. Soc.* **2002**, *149*, H12.
(22) Buijs, M.; Meyerink, A. G. *J. Lumin.* **1987**, *37*, 9.
(23) Pires, A. M.; Santos, M. F.; Davolos, M. R.; Stucchi, E. B. *J. Alloys Compd.* **2002**, *344*, 276.
(24) Guentert, O. J.; Mozzi, R. L. *Acta Crystallogr.* **1958**, *11*, 746.
(25) http://environmentalchemistry.com/yogi/periodic/ionicradius.html.

ent doping levels, synthesized by the flame pyrolysis method. The optical characterization carried out on these nanoparticles in the standard emission−excitation fluorescence measurement system, as well as a strong level of emission signal recorded from individual nanoparticles or small clusters at standard wavelengths for biological applications, in the confocal microscopy system, proves their potential for fluorescence labeling. The proportional increase of the photoluminescence emission intensity in the 5−20% range of Eu in Gd_2O_3 without observed effect of luminescence quenching, as well as a sharp narrow charge-transfer band observed in the excitation spectrum, indicates well-distributed Eu^{3+} ions without apparent Eu_2O_3 inclusions in Gd_2O_3 matrix, confirmed also by the XRD data. The synthesized nanoparticles are predominantly monoclinic as expected for our high-temperature synthesis method, but are still highly luminescent, showing intense, narrow, Stark split lines characteristic of f−f transitions at the relatively inefficient excitation at 532 nm. The most efficient excitation corresponding to the charge-transfer band between Eu^{3+} and O^{2-} ions occurs in the 230−250 nm range. The fluorescence from the cubic Eu:Gd_2O_3 nanoparticles is less susceptible to the environmental factors and a few orders of magnitude more intense than that for a monoclinic structure. The time-resolved measurements for the monoclinic Eu:Gd_2O_3 nanoparticles show a very fast component in the 2.6−3.6 ns range originating from the decay of the broad band emission from excited defect or surface states in the Gd_2O_3 matrix in all examined spectral ranges. The long decay component shows slight differences, for these ranges, in the order of hundreds of milliseconds as compared to the longest component of 3 ms observed for the strongest $^5D_0 \rightarrow {}^7F_2$ transition, in good agreement with literature reports. The cell dimensions of highly doped monoclinic Eu:Gd_2O_3 nanoparticles determined by XRD are in agreement with those previously reported for pure Gd_2O_3 powders.

Acknowledgment. This work was supported by the Australian Research Council Discovery Grant DP0451755.

JA0621602